Available online at www.sciencedirect.com
SCIENCE DIRECT®
Physica C 391 (2003) 350–362
PHYSICA C
www.elsevier.com/locate/physc

Crystalline phase development during vacuum conversion of thin barium fluoride precursor films on metallic substrates

F.A. List *, E.D. Specht, L. Heatherly, K.J. Leonard, S. Sathyamurthy, D.M. Kroeger

Metals and Ceramics Division, Oak Ridge National Laboratory, Bldg. 4500S M/S 6116, P.O. Box 2008, Oak Ridge, TN 37831-6116, USA

Received 4 March 2003; received in revised form 14 April 2003; accepted 16 April 2003

Abstract

In situ X-ray diffraction has been used to study the conversion of ~3000 Å thick, evaporated barium fluoride precursor films to YBCO on buffered metal substrates for a range of conversion time, ramp rate, water vapor pressure, oxygen pressure, and temperature. All films were taken from the same continuously processed tape. Critical current densities as high as 1.34 MA/cm^2 have been obtained for a precursor reaction rate of 2.0 Å/s. Higher reaction rates (up to 17 Å/s) lead to lower critical current densities and incompletely developed YBCO. The reaction rate increases with increasing P_{H_2O}, increasing T, and decreasing P_{O_2}. The reaction rate increases linearly with increasing P_{H_2O} for the range of pressures used here (0.0125–5.0 mTorr). The formation of non-epitaxial YBCO is generally associated with lower T and higher reaction rate, whereas the formation of barium cerate, which results from a reaction of the precursor and the CeO_2-capped substrate, is generally associated with higher T and lower reaction rate. General trends in the formation of crystalline phases during conversion may serve as a baseline for development of higher rate conversion processing for thicker, higher performance YBCO.
© 2003 Elsevier B.V. All rights reserved.

PACS: 85.25.Kx; 74.76.Bz; 81.15.Np
Keywords: YBCO; Coated conductor; Barium fluoride process; In situ X-ray diffraction

1. Introduction

Lengths of high performance $YBa_2Cu_3O_7$ (YBCO) superconducting tape have been reported by a number of laboratories throughout the world. In order for such lengths to be suitable for large-scale conductor applications, rapid and reliable processing is required throughout all stages of YBCO-coated conductor fabrication. The high performance YBCO tape from which conductor is made consists of an epitaxial YBCO film that is deposited on biaxially textured oxide buffer layers on a flexible metallic substrate [1–3]. Techniques for depositing epitaxial YBCO films include (a) direct methods such as pulsed laser deposition, in situ electron beam evaporation, and chemical vapor deposition that require no further YBCO

* Corresponding author. Tel.: +1-865-576-8020; fax: +1-865-574-7659.
E-mail address: fal@ornl.gov (F.A. List).

0921-4534/$ - see front matter © 2003 Elsevier B.V. All rights reserved.
doi:10.1016/S0921-4534(03)00965-1

processing and (b) precursor-based methods such as metal-organic deposition (MOD) and physical vapor deposition (PVD) that require further heat treatment to convert the precursor to YBCO.

Although both methods for depositing YBCO have received considerable attention, the focus of this work is on precursor-based methods. The conversion of precursor to YBCO has been studied for films deposited by both PVD [3–6] and MOD [7–9] techniques. The conversion reaction for a fluorine-based precursor can be described as:

$$\text{Y–Ba–Cu–O–F (precursor)} + H_2O \Rightarrow \text{YBCO} + 2\text{HF}.$$

Water is consumed and HF is released as the conversion proceeds. A model proposed by Solovyov et al. [6] suggests that, for atmospheric conversion, (a) the gas-phase diffusion/convection of HF away from the surface of the precursor film limits the rate of reaction and (b) the gas flow rate at the surface limits the length of conversion. These predicted limitations placed upon reaction rate and tape length for atmospheric conversion have sparked recent interest in reduced pressure conversion [10,11].

This work addresses the development of crystalline phases during reduced pressure heat treatment of YBCO precursor films. The goal is to identify processing trends and ranges of process parameters that lead to rapid and complete conversion of precursor to high performance YBCO superconductor. Although the results of this effort are strictly applicable to only the precursor (~3000 Å BaF_2 by PVD) and buffered substrate considered here, processing trends should also contribute to a baseline for comparison and development for processing of YBCO films derived from other precursor-based methods (e.g., MOD).

2. Experimental

All samples were cut to a length of 3 cm from the same continuously processed, 1-cm wide, 50-μm thick, ~1-m long tape. The tape consisted of a biaxially textured Ni–3at.%W substrate on which epitaxial buffer layers of Y_2O_3 (~200 Å), YSZ (~2500 Å), and CeO_2 (~200 Å) were deposited [12]. The Y_2O_3 was deposited at ~600 °C by electron beam evaporation of metallic yttrium in a vacuum containing $\sim 5\times10^{-5}$ Torr H_2O. The YSZ and CeO_2 were deposited at ~650 °C by magnetron R-F sputtering of oxides in the presence of $\sim 4\times10^{-5}$ Torr H_2O. Barium fluoride precursor (~3000 Å thick after conversion) was then deposited at ~100–200 °C on the buffered tape using electron beam co-evaporation of metallic yttrium, barium fluoride, and copper. The precursor thickness and cation ratio (Y:Ba:Cu = 1:2:3) were confirmed using Rutherford backscattering spectroscopy.

Each sample was spot welded to nickel leaders of cross-section similar to that of the sample and suspended between two copper water-cooled electrodes. Tension was applied to the sample with counterweights (~170 g) attached to each leader. A new, 75 μm diameter, type K thermocouple pair was spot welded to the edge of each sample to monitor substrate temperature. An electrical current through the metallic substrate was used to control the temperature of the sample. A zero crossing, phase-angle fired, 60 Hz current controller provided low thermocouple offset and noise. Linear ramp rates to the maximum conversion temperature were typically 25 °C/min and ranged from 5 to 500 °C/min. The maximum conversion temperature was varied from 620 to 770 °C. The temperature stability at the maximum conversion temperature was ~±0.5 °C, and the average quench rate following conversion was >1200 °C/min to below 200 °C.

Conversion of the BaF_2 precursor to YBCO was accomplished in an all-metal sealed, hydrocarbon-free, vacuum chamber. A base pressure of $\sim 5\times10^{-7}$ Torr was attained after a pump down of ~2 h. A quadrupole mass spectrometer revealed that water vapor was the major component of the residual gas. During conversion, the partial pressures of oxygen and water vapor were controlled with manual precision leak valves. The water vapor pressure (generally 0.01–5 mTorr) was first established using either a capacitance diaphragm manometer (for pressures $\geqslant$ 0.5 mTorr) or a cold cathode ionization gauge (for pressures < 0.5

mTorr). Next the partial pressure of oxygen (generally 10–200 mTorr) was established using the capacitance diaphragm manometer. During conversion, the oxygen leak valve was manually adjusted to maintain the desired total pressure. After conversion, the oxygen leak valve was closed and the water vapor pressure was checked for drift throughout the conversion. Drift of the water vapor pressure was found to be typically <±10%.

Energy dispersive X-ray (EDX) diffraction continuously monitored the development of crystalline phases during precursor conversion. A Bragg–Brentano parafocusing geometry was used. A fixed tungsten anode with a 1×10 mm^2 source and a 5° take-off angle provided an effective source size of 0.1×10 mm^2, and a receiving slit of dimension 1×10 mm^2 was used. Both the source and the receiving slit were 30 cm from the sample. The incident and diffracted X-rays were at a fixed glancing angle of 5°. Soller slits limited the axial divergence of both the incident and diffracted X-rays to 2°. An energy dispersive, liquid nitrogen cooled Ge detector was used; the energy resolution of the detector was the limiting factor in instrumental resolution. Beryllium windows, 250-μm thick, allowed X-rays to pass through the walls of the vacuum conversion chamber. The X-ray tube was operated at 40 kV and 30 mA; 40 kV was chosen to avoid exciting the Ni(2 0 0) reflection, which would otherwise saturate the detector.

Fig. 1a shows an X-ray spectrum for a converted sample obtained in 20 min with the EDX system. For comparison, Fig. 1b shows an X-ray spectrum for the same sample obtained in the same time with a standard θ–2θ diffractometer using a 50 kV, 30 mA copper anode and a scintillation detector. Although both spectra show similar diffraction features, the EDX spectrum shows lower 2θ resolution and fluorescence peaks. The two major advantages of this EDX system are its simplicity (no moving components) and the fact that spectra are collected simultaneously for the full range of 2θ. Scanning dead time, timing offset, and failure to monitor unexpected peaks are thus reduced. Throughout precursor conversion, EDX diffraction spectra were recorded continuously and stored every two minutes for each sample. Following conversion, standard θ–2θ spectra were recorded for each sample using monochromatic CuK$_\alpha$ radiation.

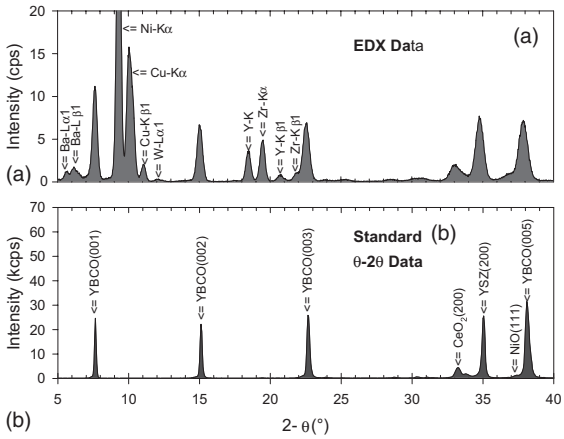

Fig. 1. X-ray spectra obtained in 20 min for the same fully converted YBCO film. (a) EDX spectrum showing CuK$_\alpha$ equivalent 2θ. (b) X-ray spectrum obtained with a standard θ–2θ diffractometer using a 50 kV, 30 mA copper anode.

Transport critical current (I_c) was measured in liquid nitrogen (~77 K) and self-field using the standard four-probe technique with a voltage probe spacing of 0.4 cm and a 1 μV/cm criterion for I_c. Prior to I_c measurements, samples were sputter deposited with silver (~1 μm thick) for electrical contacts and oxygenated at 510 °C in flowing pure oxygen at 1 atm for 60 min.

3. Results

Conversion of BaF_2 precursor to YBCO generally involves thermally ramping the precursor to an elevated temperature (typically ~740 °C) in the presence of oxygen and water vapor and maintaining that temperature for a time sufficient for conversion to complete. Oxygen is required for thermodynamic stability of the YBCO, and water vapor participates in the removal of fluorine from the precursor. Process parameters investigated in this work include conversion time, ramp rate, water vapor pressure, oxygen pressure, and temperature. All processing has been conducted in the absence of a carrier gas; the total pressure during processing is the sum of the partial pressures of

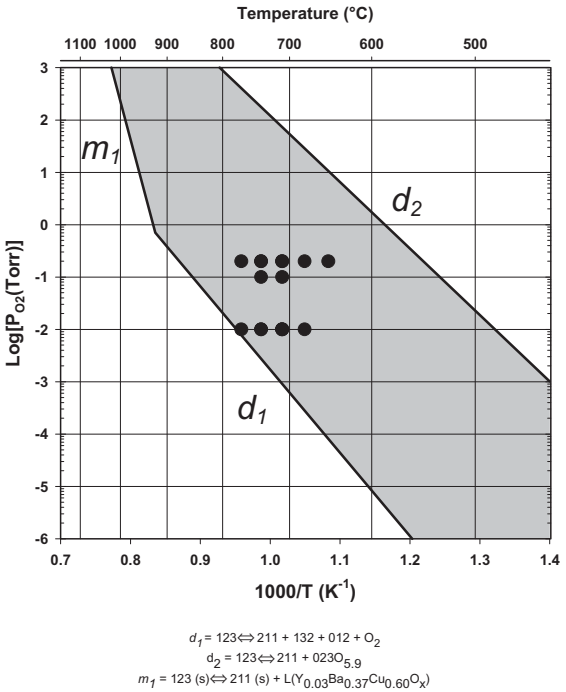

Fig. 2. Distribution of temperatures and oxygen partial pressures used for this precursor conversion study. YBCO is stable in the shaded area.

oxygen and water. Gas purity has been confirmed with in situ mass spectrometry.

Fig. 2 shows the distribution of temperatures and oxygen partial pressures used for this precursor conversion study. Also shown are several thermodynamic stability lines determined for YBCO [4,13]. A plot of this kind is useful when selecting conversion temperatures and oxygen partial pressures for which YBCO, if formed during the conversion, is stable. The shaded area represents the region of temperature-P_{O_2} space in which YBCO is stable. To clarify, the shaded area does not represent the region of temperature-P_{O_2} space in which precursor will necessarily convert to YBCO; such a region depends on additional factors such as the thermodynamics and kinetics of alternative chemical pathways. The ranges of conversion time, ramp rate and water vapor pressure used in this investigation are also not shown in Fig. 2.

The rate at which epitaxial YBCO grows, G, is of central importance for understanding and accelerating precursor conversion. Both X-ray diffraction [8] and in situ electrical conductance [14] methods have been used to estimate G during precursor conversion. McIntyre et al. [8] have used the ratio of the integrated intensity of an epitaxial YBCO X-ray peak for a partially converted film to that for a fully converted film as a quantitative measure of the volume fraction of epitaxial YBCO. The accuracy of an estimate of G using this X-ray method depends on whether the fully converted film is (a) indeed fully epitaxial YBCO and (b) comparable in properties (e.g., final thickness and crystalline texture) to the partially converted film. Similarly, Solovyov et al. [14] have used the ratio of the instantaneous electrical conductance to the final electrical conductance achieved after a long conversion time as a measure of the extent of epitaxial YBCO formation. The accuracy of an estimate of G using this conductance method depends on how accurately the final electrical conductance represents that for a fully epitaxial YBCO film.

For this study, the ratio of the intensity of the epitaxial YBCO(0 0 2) EDX peak for a partially converted film to that for a fully converted film has been used as a measure of the extent of epitaxial YBCO formation. The product of the time derivative of this ratio and the final thickness of the fully converted film (3000 Å) has been used to estimate G, the growth rate of epitaxial YBCO. For some conversion conditions, the maximum intensity of the YBCO(0 0 2) peak is less than the intensity for a fully converted film. This suggests that for these conditions the fully reacted film has not converted fully to epitaxial YBCO. The ratio of the instantaneous intensity to the maximum intensity of the YBCO(0 0 2) EDX peak for a particular film during conversion has been used as a measure of the extent of precursor reaction. The product of the time derivative of this ratio and the final thickness of the fully converted film (3000 Å) has been used to estimate G_p, the reaction rate of the precursor. For a film that fully converts to epitaxial YBCO, the estimated values for G and G_p are roughly equal throughout the conversion process. However, for a film that does not fully convert to epitaxial YBCO, the estimate for G is generally less than that for G_p.

3.1. Variable conversion time

Fig. 3 shows EDX results obtained for five precursor samples for which the time at conversion temperature was varied. Times were varied from 15 to 180 min. Samples were heated using a linear ramp rate of 25 °C/min from ~20 to 740 °C in 200 mTorr oxygen and 0.5 mTorr water. The X-ray intensity for YBCO(0 0 2) ($d = 5.85$ Å) develops during conversion similarly for all times. At approximately the time at which 740 °C is first reached (time = 0 min in Fig. 3a), the YBCO(0 0 2) intensity begins to rise at a rate which is roughly linear with respect to time. If the YBCO(0 0 2) intensity is assumed to be proportional to the amount of YBCO present, this linear rate of rise would suggest a roughly constant YBCO growth rate. Solovyov et al. [6,14] using conductance measurements during atmospheric PVD precursor conversion and Smith et al. [9] using in situ X-ray diffraction during atmospheric MOD precursor conversion have both similarly observed constant YBCO growth rates. After ~25 min at 740 °C, this linear rate of rise abruptly decreases and the YBCO(0 0 2) intensity continues to increase at a lower rate for the remainder of the conversion time. Smith et al. [9] have reported nearly identical behavior for MOD conversion at 735 °C. If the measured YBCO(0 0 2) intensity at the knee (at time = ~25 min) is assumed to represent complete conversion (~3000 Å YBCO), the growth rate of epitaxial YBCO (G) can be estimated from the slope to be 2.0 Å/s.

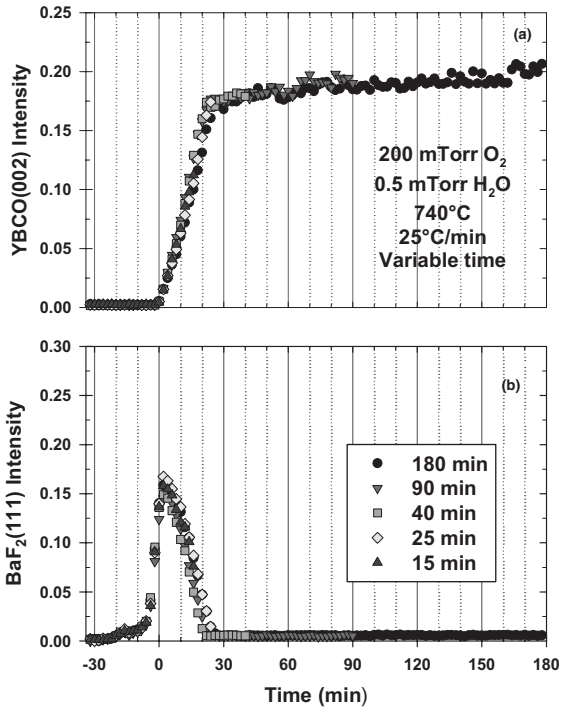

Fig. 3. EDX results obtained for five precursor samples for variable time at conversion temperature.

To assess the crystalline quality of the YBCO, (1 1 3) pole figures, (1 1 3) ϕ-scans, and (0 0 2) ω-scans were obtained for each sample in Fig. 3 following conversion. Both the in-plane and out-of-plane textures for YBCO were found to be independent of conversion time and equal to $6.7 \pm 0.2°$ and $4.26 \pm 0.06°$ FWHM, respectively. Pole figure analysis revealed 87.4% cube textured YBCO for the 15 min conversion time and $93.2 \pm 0.2\%$ cube textured YBCO for all other conversion times. Improvements in YBCO crystalline quality are not detectable for conversion times greater than 25 min where Fig. 3a shows the lower rate of rise of YBCO(0 0 2) intensity.

Unlike the X-ray intensity for YBCO(0 0 2), the BaF_2(1 1 1) ($d = 3.58$ Å) intensity develops during the initial temperature ramp, is a maximum within ~2 min after first reaching 740 °C, and decays to zero after ~25 min at 740 °C (see Fig. 3b). This behavior is again nearly identical to that observed by Smith et al. [9] for atmospheric conversion of MOD precursor. Wu et al. [15] have suggested that a crystalline oxy-fluoride phase ($Y_{0.3}Ba_{0.7}$-$(O_{0.15}F_{0.85})_2$), having a crystal structure and lattice parameter that are indistinguishable from those of barium fluoride, plays a key role during the precursor conversion to YBCO. The X-ray intensity we attribute to barium fluoride may include a contribution from this oxy-fluoride phase.

Fig. 4 shows the θ–2θ X-ray peak areas for YBCO(0 0 2) and BaF_2(1 1 1) and the I_c as a function of total conversion time; all were obtained after conversion. Uniformly high I_c is obtained for a significant range of conversion time (25–180 min). In contrast, for atmospheric conversion high I_c is frequently obtained for a rather

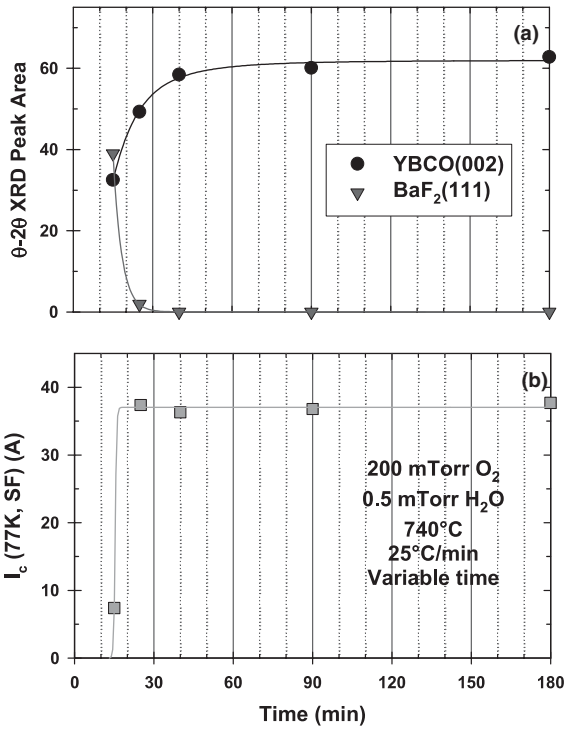

Fig. 4. θ–2θ X-ray peak areas for YBCO(0 0 2) and BaF_2(1 1 1) and the I_c obtained after conversion as a function of total conversion time.

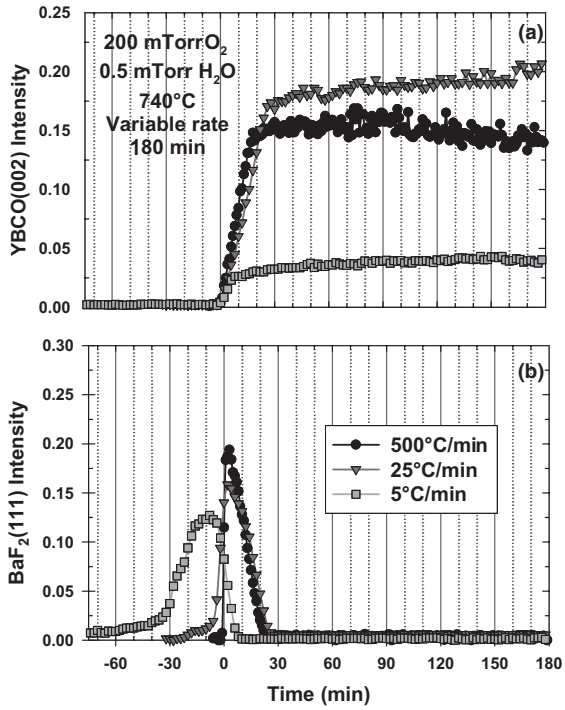

Fig. 5. EDX results obtained for three linear ramp rates (5, 25, and 500 °C/min).

narrow range of conversion time with decreased I_cs obtained for conversion times beyond this range. This degradation of I_c has been attributed to YBCO back-reaction with HF [16] and water. Back-reaction appears to be less of a problem for reduced pressure precursor conversion. An I_c of 37.4 A (corresponding to a J_c of 1.34 MA/cm^2) is exhibited for the sample converted for only 25 min. X-ray diffraction for this 25 min sample shows less than fully developed YBCO and some unreacted BaF_2.

3.2. Variable ramp rate

EDX results are shown as a function of time for three linear ramp rates (5, 25, and 500 °C/min) in Fig. 5. Again, time = 0 min is the time at which the conversion temperature is first reached. For these results, conversion temperature is 740 °C, time at conversion temperature is 180 min, oxygen pressure is 200 mTorr and water vapor pressure is 0.5 mTorr. No crystalline YBCO(0 0 2) is detectable for all ramp rates before 740 °C is first reached. For the 5 and 500 °C/min ramp rates, the YBCO(0 0 2) intensity never develops fully. This may suggest that the quantity and/or crystalline quality of epitaxial YBCO are underdeveloped for these ramp rates. Also, crystallization of BaF_2 begins for all ramp rates before 740 °C is first reached. Only for the slowest ramp rate (5 °C/min) does the BaF_2(1 1 1) intensity begin to decay both before 740 °C is reached and before any crystalline YBCO(0 0 2) is detectable.

Fig. 6a shows the θ–2θ X-ray peak areas for YBCO(0 0 2), $BaCeO_3$(1 1 0), NiO(1 1 1), and YBCO(1 0 3) obtained after conversion as a function of ramp rate. No BaF_2(1 1 1) peak is detectable after conversion for any ramp rate. The lower YBCO(0 0 2) intensity observed for 5 °C/min is accompanied by significant NiO(1 1 1) and random YBCO(1 0 3), whereas the lower YBCO(0 0 2)

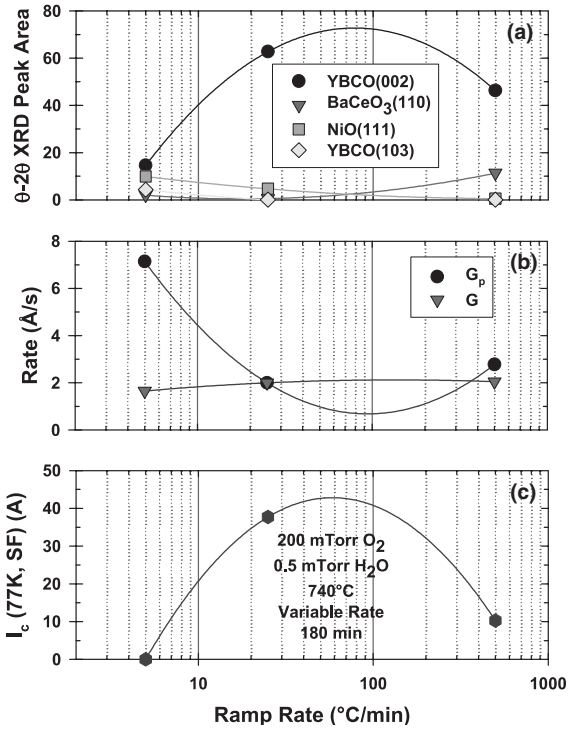

Fig. 6. Additional results obtained for three linear ramp rates. (a) θ–2θ X-ray peak areas for YBCO(0 0 2), $BaCeO_3$(1 1 0), NiO(1 1 1), and YBCO(1 0 3) obtained after conversion as a function of ramp rate. (b) Estimated precursor reaction rate and YBCO growth rate as a function of ramp rate. (c) I_c measured at 77 K and self-field as a function of ramp rate.

intensity observed for 500 °C/min is accompanied by significant $BaCeO_3$(1 1 0)—an indication of a reaction of the precursor with CeO_2 in the substrate. Higher ramp rates might be expected to result in the formation of more chemically reactive liquid phase and, thus, more substrate reaction [11]. Fig. 6b shows the estimated precursor reaction rate, G_p, and epitaxial YBCO growth rate, G, as a function of ramp rate. Values for G_p and G are time averaged for times ranging from zero to the time at which the knee for the YBCO(0 0 2) intensity is reached. Note that for 5 °C/min, the value of G_p is nearly four times that of G; this may be a reflection of a conversion process that is dominated by a rapid precursor reaction to form random, non-epitaxial YBCO. Fig. 6c shows the I_c measured for each sample at 77 K and self-field. The I_c is higher and the G_p is lower for 25 °C/min than for those for both 5 and 500 °C/min.

3.3. Variable P_{H_2O}

Fig. 7 shows EDX results obtained as a function of time for five water vapor partial pressures. The oxygen partial pressure, conversion temperature, ramp rate and conversion time are constant and 200 mTorr, 740 °C, 25 °C/min, and 180 min, respectively. As the P_{H_2O} increases, the times decrease for YBCO(0 0 2) to develop and BaF_2(1 1 1) to decay. For the higher P_{H_2O} (3.0 and 5.0 mTorr), the YBCO(0 0 2) intensity does not develop fully. The maximum intensity for BaF_2(1 1 1) is substantially greater for low P_{H_2O} than for high P_{H_2O}. This is likely a consequence of the relationship between the rate of crystalline BaF_2 formation and the rate of BaF_2 consumption through precursor reaction. Low precursor reaction rate at low P_{H_2O}

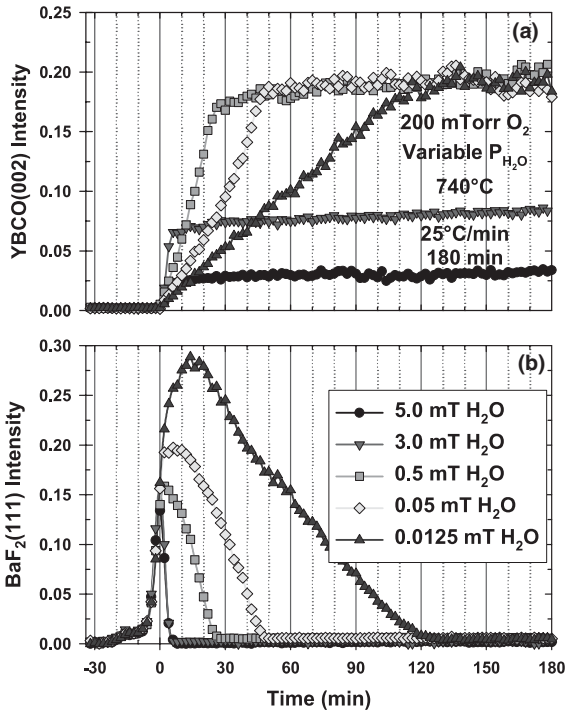

Fig. 7. EDX results obtained at 200 mTorr O_2 and 740 °C for five water vapor partial pressures.

is associated with low BaF_2 consumption and a temporary build-up of crystalline BaF_2.

Fig. 8 shows θ–2θ X-ray peak areas, precursor reaction rate, epitaxial YBCO growth rate, and critical current as a function of P_{H_2O} for these five samples. For $P_{H_2O} = 0.5$ mTorr, the YBCO(0 0 2) peak area and I_c are a maximum and the NiO(1 1 1) and $BaCeO_3$(1 1 0) peak areas are a minimum. For the highest conversion rate (~12.5 Å/s and $P_{H_2O} = 5$ mTorr), randomly oriented YBCO(1 0 3) is detected and may arise from insufficient atomic mobility for epitaxy during YBCO formation. For the lowest conversion rate (~0.3 Å/s and $P_{H_2O} = 0.0125$ mTorr), $BaCeO_3$(1 1 0) is evident which implies a precursor/substrate reaction during the protracted conversion.

The inset for Fig. 8b shows that for this range of P_{H_2O}, the precursor reaction rate depends linearly on water vapor partial pressure. This is consistent with a conversion reaction that is limited in rate by the supply of water from the gas phase to the conversion surface. A $(P_{H_2O})^{1/2}$ dependence of conversion rate observed for somewhat higher ranges of P_{H_2O} [10,14] has been attributed to a conversion reaction that is limited by HF removal by means of gaseous diffusion and convection [6]. The removal of HF does not appear to be conversion rate limiting for this low range of pressure. The non-zero precursor reaction rate suggested by extrapolation to $P_{H_2O} = 0$ in Fig. 8b inset is believed to be a consequence of the presence of elevated P_{H_2O} associated with water desorption from the vacuum chamber walls during sample heating.

Figs. 9 and 10 show results that are similar to those of Figs. 7 and 8 obtained for an oxygen partial pressure of 10 mTorr and a conversion temperature of 710 °C. For all P_{H_2O}, the values of G_p and G are higher and the I_cs are generally lower for conditions of low conversion temperature and P_{O_2} (710 °C and 10 mTorr) than for high

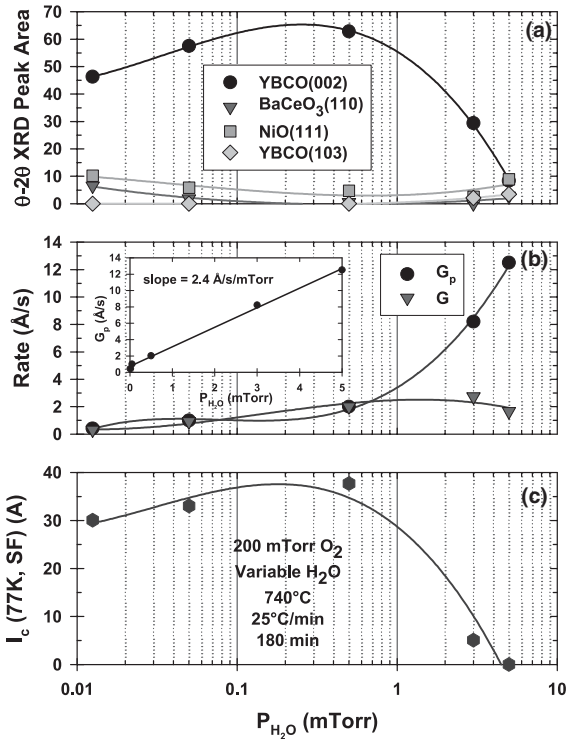

Fig. 8. θ–2θ X-ray peak areas, precursor reaction rate, YBCO growth rate, and critical current as a function of P_{H_2O} for 200 mTorr O_2 and 740 °C.

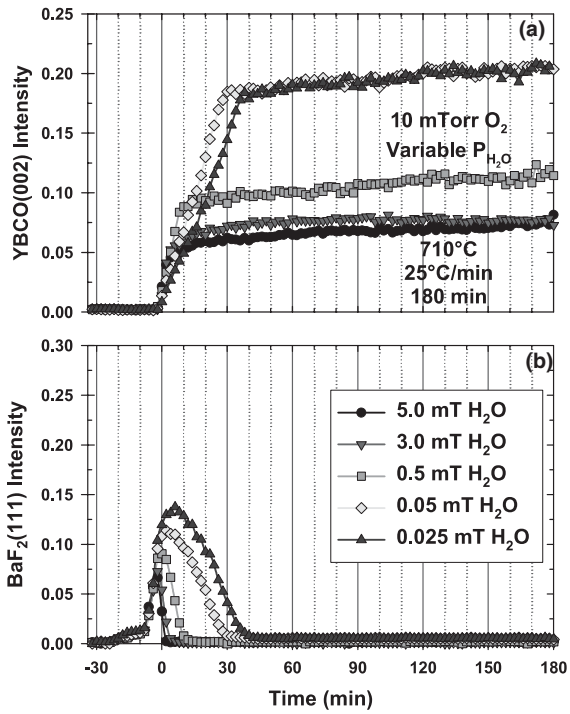

Fig. 9. EDX results obtained at 10 mTorr O_2 and 710 °C for five water vapor partial pressures.

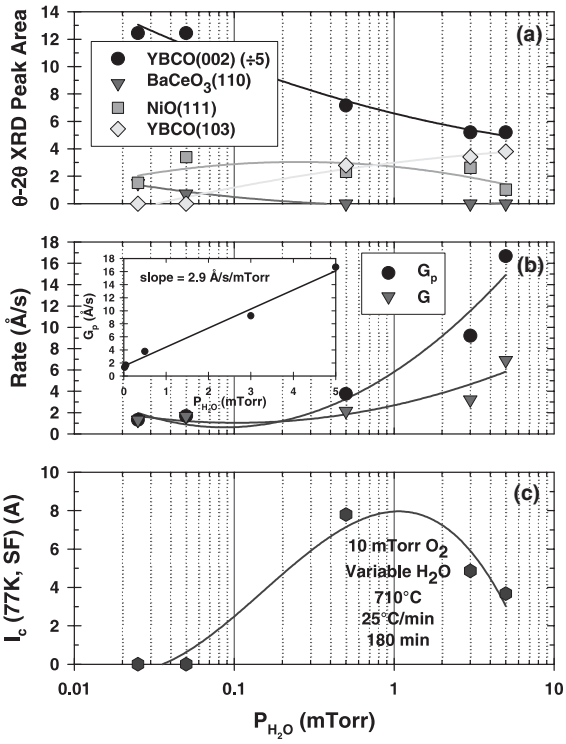

Fig. 10. θ–2θ X-ray peak areas, precursor reaction rate, YBCO growth rate, and critical current as a function of P_{H_2O} for 10 mTorr O_2 and 710 °C.

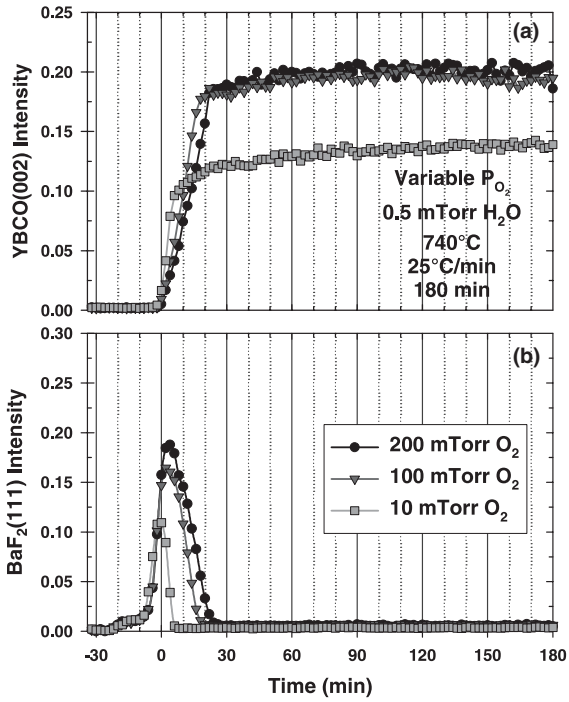

Fig. 11. EDX results obtained at 740 °C for three oxygen partial pressures.

conversion temperature and P_{O_2} (740 °C and 200 mTorr). Also for high values of G_p (~4 Å/s and greater), randomly oriented YBCO(1 0 3) is detected. Low I_c is associated with a detectable $BaCeO_3$(1 1 0) intensity and low G_p. Compared to the slope of the line in Fig. 8b inset for 740 °C conversion (2.4 Å/s/mTorr), the slope in Fig. 10b inset for 710 °C conversion (2.9 Å/s/mTorr) is higher. A lower sticking coefficient (i.e., adsorption probability) for water at higher temperature may account for this difference in slopes.

3.4. Variable P_{O_2}

EDX results are shown as a function of time for three oxygen partial pressures (10, 100, and 200 mTorr) in Fig. 11. The water vapor partial pressure, conversion temperature, ramp rate and conversion time are constant and 0.5 mTorr, 740 °C, 25 °C/min, and 180 min, respectively. For the lowest P_{O_2} (10 mTorr), the YBCO(0 0 2) intensity develops incompletely (i.e., to a final intensity in Fig. 11a of less than ~0.21). Fig. 12 shows θ–2θ X-ray peak areas, G_p, G, and critical current as a function of P_{O_2} for these three samples. For this range of P_{O_2}, the values of G_p and G decrease and the critical current increases as P_{O_2} increases. Lower cation mobility in the oxide precursor resulting from fewer oxygen vacancies at higher P_{O_2} may lead to lower G_p and G at higher P_{O_2} [4]. Low I_c for $P_{O_2} = 10$ mTorr is associated with detectable $BaCeO_3$ (1 1 0) and random YBCO(1 0 3) intensities.

Figs. 13 and 14 show results that are similar to those of Figs. 11 and 12 except the conversion temperature is 710 °C. For all P_{O_2}, the YBCO(0 0 2) intensity develops incompletely—never reaching an intensity of ~0.21. The presence of substantial YBCO(2 0 0) X-ray intensity (a-axis perpendicular or $a\perp$YBCO) for 200 mTorr oxygen accompanies a zero critical current. Observation of $a\perp$YBCO for this oxygen partial pressure and conversion

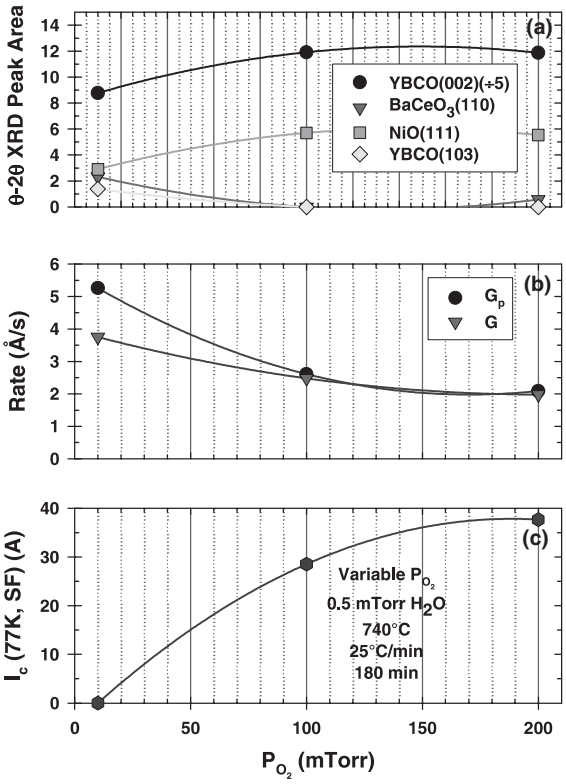

Fig. 12. θ–2θ X-ray peak areas, precursor reaction rate, YBCO growth rate, and critical current as a function of P_{O_2} at 740 °C.

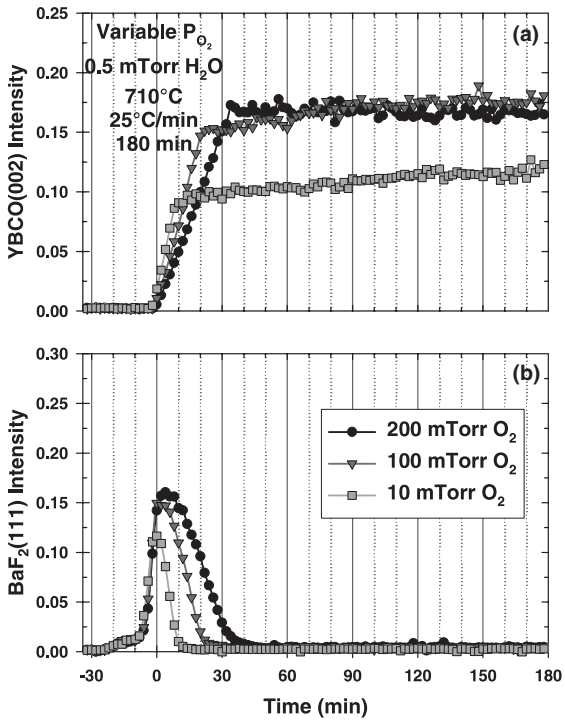

Fig. 13. EDX results obtained at 710 °C for three oxygen partial pressures.

temperature is in qualitative agreement with result of Feenstra et al. [4] for atmospheric conversion. For all P_{O_2}, values of G_p and G are higher for higher conversion temperature (compare Figs. 12b and 14b).

3.5. Variable T

Fig. 15 shows EDX results obtained as a function of time for five conversion temperatures. The oxygen partial pressure, water vapor partial pressure, ramp rate and conversion time are 200 mTorr, 0.05 mTorr, 25 °C/min, and 210–270 min, respectively. The total conversion times for these samples are extended to ensure complete conversion. Fig. 16 shows θ–2θ X-ray peak areas, G_p, G, and critical current as a function of conversion temperature for these five samples. For this range of temperature, G_p and G increase as conversion temperature increases. A similar observation was made above (Figs. 11–14) for variable oxygen partial pressure at 740 and 710 °C. Low critical current, high NiO(1 1 1), and high YBCO(2 0 0) ($a\perp$YBCO) are observed after conversion at low conversion temperatures. Again, observation of $a\perp$YBCO for this oxygen partial pressure and conversion temperature is in qualitative agreement with result of Feenstra et al. [4] for atmospheric conversion. For high conversion temperature, low critical current and elevated $BaCeO_3$(1 1 0) are observed.

Fig. 17 shows EDX results obtained as a function of time for four conversion temperatures. The oxygen partial pressure, water vapor partial pressure, ramp rate and conversion time are 10 mTorr, 0.5 mTorr, 25 °C/min, and 180 min, respectively. Fig. 18 shows θ–2θ X-ray peak areas, G_p, G, and critical current as a function of conversion temperature for these four samples. For this range of temperature, G_p and G generally increase as

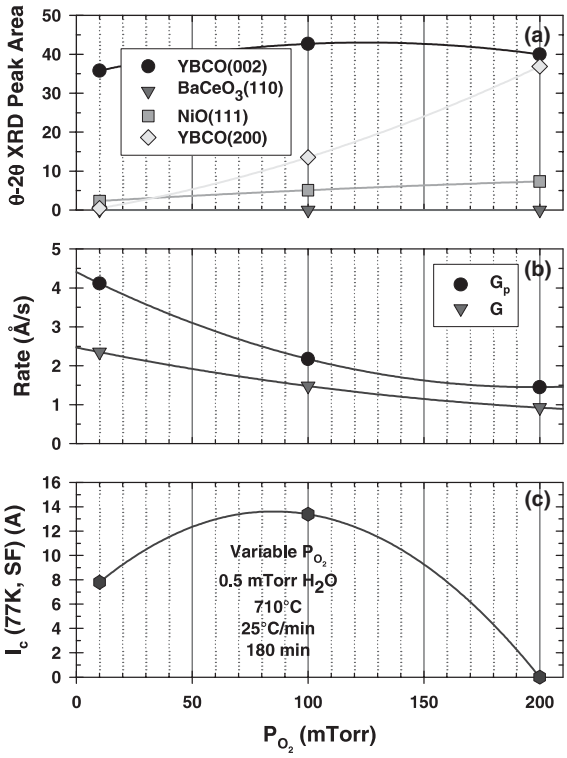

Fig. 14. θ–2θ X-ray peak areas, precursor reaction rate, YBCO growth rate, and critical current as a function of P_{O_2} at 710 °C.

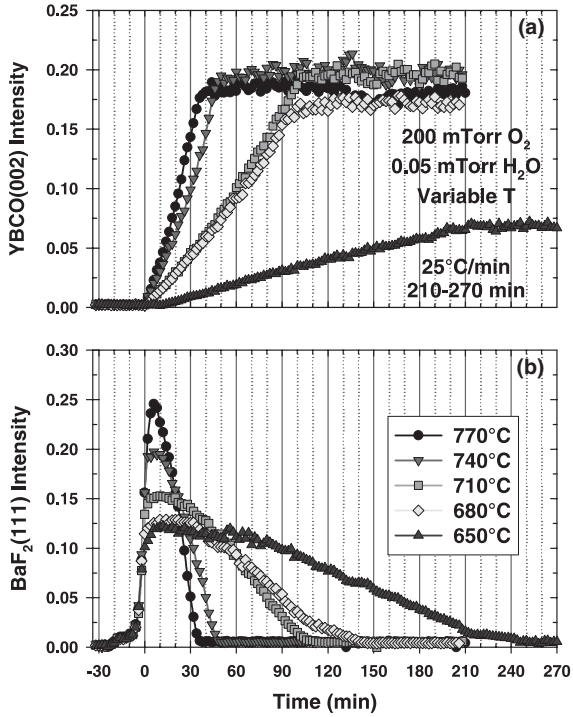

Fig. 15. EDX results obtained at 200 mTorr O_2 and 0.05 mTorr H_2O for five conversion temperatures.

conversion temperature increases and the development of YBCO(0 0 2) intensity is incomplete. For 740 °C, low critical current and detectable $BaCeO_3$(1 1 0) are observed. For 770 °C, low G, low critical current, and high $BaCeO_3$(1 1 0) are observed. Also for 770 °C, the EDX intensity for YBCO(0 0 2) reaches a maximum and then decreases with further conversion time (Fig. 18a). This apparent decomposition of YBCO is likely related to the proximity of 770 °C and 10 mTorr P_{O_2} to the YBCO stability line (see Fig. 2).

4. Discussion and conclusions

From the results presented above, several general trends for conversion for this precursor/substrate combination and this range of processing parameters can be identified. The precursor conversion rate (G_p) and the epitaxial YBCO growth rate (G) have been estimated from the YBCO(0 0 2) X-ray intensity and range from ~0.2 to ~17 Å/s and ~0.06 to ~7 Å/s, respectively. Both are roughly constant throughout the conversion process and generally increase with increasing P_{H_2O}, increasing T, and decreasing P_{O_2}. High performance YBCO (I_c >~30 A; J_c >~1.07 MA/cm^2) develops for G_p and G ranging from 0.2 to 2.5 Å/s, with the best I_cs (~37 A) obtained for G_p and G ranging from ~1.0 to ~2.0 Å/s. High G_p (>~3 Å/s) samples exhibit low performance (I_c < 10 A) and less than fully developed YBCO(0 0 2) intensity.

Low I_c is frequently accompanied by the formation of non-epitaxial YBCO or barium cerate. The formation of non-epitaxial YBCO, which is evident from YBCO(1 0 3) X-ray intensity, is generally associated with lower T and higher G_p (>~4 Å/s). High conversion temperature and long conversion time (low G_p) lead to adequate atomic mobility for the formation of high quality epitaxial

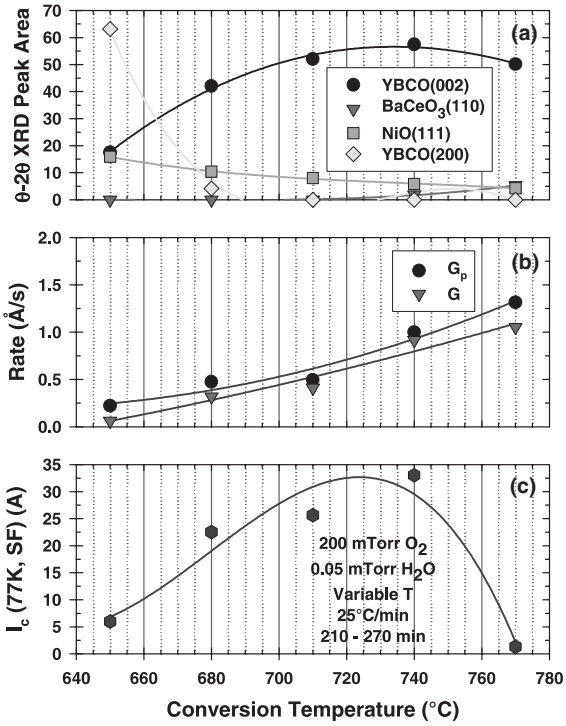

Fig. 16. θ–2θ X-ray peak areas, precursor reaction rate, YBCO growth rate, and critical current as a function of conversion temperature at 200 mTorr O_2 and 0.05 mTorr H_2O.

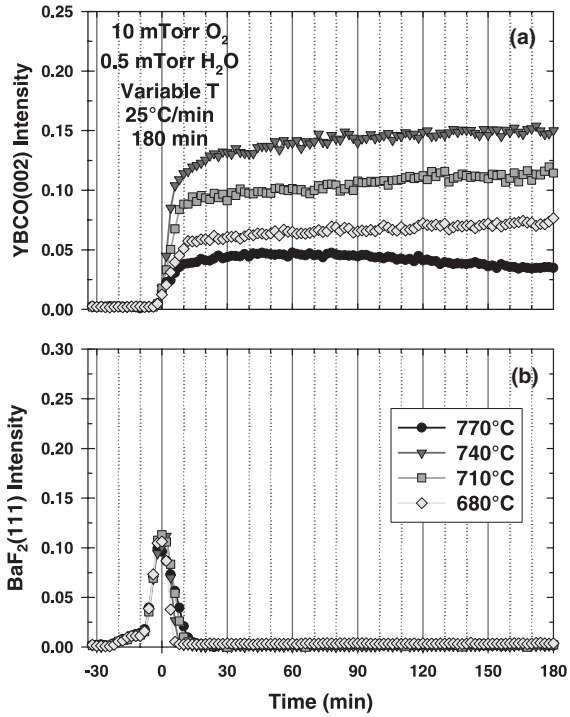

Fig. 17. EDX results obtained at 10 mTorr O_2 and 0.5 mTorr H_2O for four conversion temperatures.

YBCO. The formation of barium cerate, which results from a reaction of the precursor and the CeO_2-capped substrate, is generally associated with higher T and lower G_p. Low conversion temperature and short conversion time (high G_p) represent favorable conditions for substrate stability. These trends in crystalline phase development appear to place an upper limit on G_p (and G) for a particular precursor/substrate combination that lead to high I_c YBCO. Increasing T to exceed this upper limit on G_p results in substrate reaction, and increasing P_{H_2O} to exceed this limit results in poor epitaxy.

Attempts to achieve higher values of G_p and G while maintaining high I_c include those of Yoshizumi et al. [11] who have recently used fluorine-rich MOD precursor with high ramp rate (~380 °C/min) and low total pressure to promote the formation of liquid phases, and hence the intrinsic atomic mobility, during conversion at 785 °C. Conversion rates of >60 Å/s and $J_c = 1.7$ MA have been reported. The presence of fluorine-rich liquid phases at higher temperature, however, may place greater demand on substrate stability. Another approach to achieving higher G_p is to develop buffer layers that are more chemically resistant and more compatible with high temperature, high rate processing. Such buffer layers might include those terminated with epitaxially compatible oxides other than CeO_2, such as $SrRuO_3$ [17].

In situ X-ray diffraction provides a powerful tool for studying kinetics of crystalline phase development. Barium fluoride precursor conversion to YBCO for a ~3000 Å thick precursor deposited by electron beam evaporation has been systematically studied using in situ X-ray diffraction for a wide range of processing parameters. Conversion kinetics, chemical pathways, and I_c performance show strong dependence on all processing parameters. Processing trends identified here provide

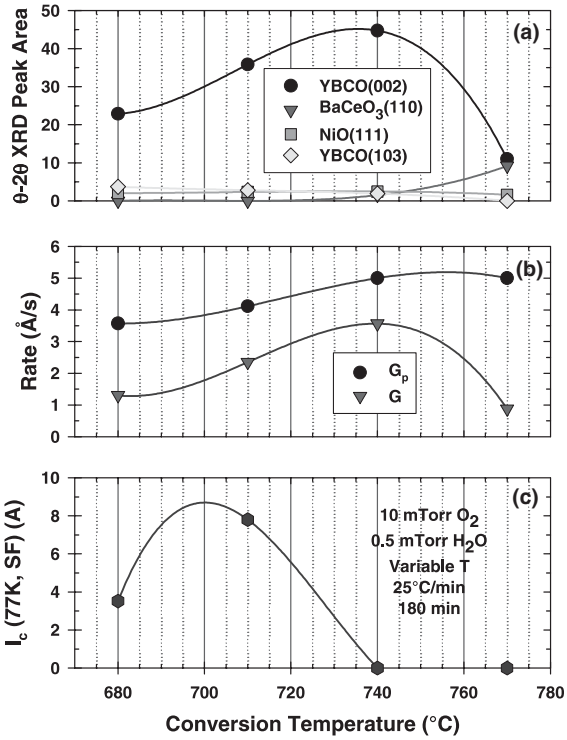

Fig. 18. θ–2θ X-ray peak areas, precursor reaction rate, YBCO growth rate, and critical current as a function of conversion temperature at 10 mTorr O_2 and 0.5 mTorr H_2O.

tools for the design and perhaps understanding of large scale, high rate precursor processing.

Acknowledgements

Research sponsored by the United States Department of Energy, Office of Energy Efficiency and Renewable Energy, Office of Distributed Energy and Electric Reliability—Superconductivity program. This research was performed at the Oak Ridge National Laboratory, managed by UT-Battelle, LLC for the United States Department of Energy under contract no. DE-AC05-00OR22725.

References

[1] X.D. Wu, S.R. Foltyn, P.N. Arendt, W.R. Blumenthal, I.H. Campbell, J.D. Cotton, J.Y. Coulter, W.L. Hults, M.P. Maley, H.F. Safar, J.L. Smith, Appl. Phys. Lett. 67 (1995) 2397.

[2] K. Hasegawa, N. Yoshida, K. Fujino, H. Mukai, K. Hayashi, K. Sato, Y. Sato, S. Honjo, T. Ohkuma, H. Ishii, T. Hara, in: S. Nakajima, M. Murakami (Eds.), Advances in Superconductivity IX, Proceedings of the 9th International Symposium on Superconductivity (ISS'96), Sapporo, Japan, 1996, p. 745.

[3] A. Goyal, D.P. Norton, J.D. Budai, M. Paranthaman, E.D. Specht, D.M. Kroeger, D.K. Christen, Q. He, B. Saffian, F.A. List, D.F. Lee, P.M. Martin, C.E. Klabunde, E. Hatfield, V.K. Sikka, Appl. Phys. Lett. 69 (1996) 1795.

[4] R. Feenstra, T.B. Lindemer, J.D. Budai, M.D. Galloway, J. Appl. Phys. 69 (1991) 6569.

[5] M.P. Siegal, J.M. Phillips, R.B. van Dover, T.H. Tiefel, J.H. Marshall, J. Appl. Phys. 68 (1990) 6353.

[6] V.F. Solovyov, H.J. Weismann, M. Suenaga, Physica C 353 (2001) 14.

[7] P.C. McIntyre, M.J. Cima, J. Mater. Res. 9 (1994) 2219.

[8] P.C. McIntyre, M.J. Cima, A. Roshko, J. Appl. Phys. 77 (1995) 5263.

[9] J.A. Smith, M.J. Cima, N. Sonnenberg, IEEE Trans. Appl. Supercond. 9 (1999) 1531.

[10] V.F. Solovyov, H.J. Weismann, L.-J. Wu, Y. Zhu, M. Suenaga, IEEE Trans. Appl. Supercond. 11 (2001) 2939.

[11] M. Yoshizumi, I. Seleznev, M.J. Cima, Symposium S, S8.11, Mater. Res. Soc. 2002 Fall Meeting, Boston, MA.

[12] A. Goyal, R. Feenstra, M. Paranthaman, J.R. Thompson, B.Y. Kang, C. Cantoni, D.F. Lee, F.A. List, P.M. Martin, E. Lara-Curzio, C. Stevens, D.M. Kroeger, M. Kowalewski, E.D. Specht, T. Aytug, S. Sathyamurthy, R.K. Williams, R.E. Ericson, Physica C 382 (2002) 251.

[13] R.H. Hammond, R. Bormann, Physica C 162–164 (1989) 162.

[14] V.F. Solovyov, H.J. Weismann, L.-J. Wu, Y. Zhu, M. Suenaga, Appl. Phys. Lett. 76 (2000) 1911.

[15] L. Wu, Y. Zhu, V.F. Solovyov, H.J. Wiesmann, A.R. Moodenbaugh, R.L. Sabatini, M. Suenaga, J. Mater. Res. 16 (2001) 2869.

[16] V.F. Solovyov, H.J. Wiesmann, M. Suenaga, Symposium S, S4I-1, 2001 International Workshop on Superconductivity, ISTEC and Mater. Res. Soc. Co-sponsored, Honolulu, Hawaii.

[17] Q.X. Jia, S.R. Foltyn, P.N. Arendt, J.R. Groves, T.G. Holesinger, M.E. Hawley, P. Lu, Appl. Phys. Lett. 81 (2002) 4571.